Structural crossover in dense irreversibly aggregating particulate systems

D. Fry,* A. Chakrabarti, W. Kim, and C. M. Sorensen
Department of Physics, Cardwell Hall, Kansas State University, Manhattan, Kansas 66506-2601, USA
(Received 9 October 2003; published 1 June 2004)

Cluster-cluster aggregation has been simulated by off-lattice Monte Carlo methods for diffusion-limited (DLCA), ballistic-limited, and reaction-limited cluster aggregation classes. We find that as the system evolves and becomes dense, the largest cluster develops a hybrid structure with mass fractal dimension $D_f \simeq 2.6$ over large length scales, while at smaller length scales, the early time dilute-limit fractal structure is frozen in. The largest cluster is thus an aggregate of smaller aggregates with a different fractal dimension, and we call it a "superaggregate." The crossover length separating the two morphologies, which we call the critical radius of gyration, can be calculated based on a simple theory that assumes a monodisperse cluster size distribution. This agrees well with simulation results for DLCA. However, for other classes we find that the increasing polydispersity in cluster size pushes the simulated crossover length radius of gyration to values systematically larger than the predicted value.

DOI: 10.1103/PhysRevE.69.061401 PACS number(s): 82.70.Gg, 82.70.Rr

I. INTRODUCTION

The sol-gel transition has been extensively studied by both chemists and physicists. Aggregation in a dilute sol has been well understood since the early part of the last century, while percolation theory has been widely used throughout the past three decades to describe both the transition to a dense state and the gel itself. For instance, shear viscosity and elastic moduli, relaxation times, and both long and short time diffusion coefficients of colloidal and polymeric systems show behavior near the sol-gel transition point reminiscent of critical phenomena usually associated with percolation [1]. However, the details of the evolution from dilute to crowded, is largely unknown. As a first step toward understanding this evolution, we have recently carried out large-scale off-lattice Monte Carlo (OLMC) simulations [2] of the *kinetics* of diffusion-limited cluster aggregation (DLCA) over the entire range of evolution of the system—from dilute to crowded. The goal of the present paper is to provide a coherent description of the *morphological changes* that takes place as the system evolves from the dilute to the crowded state.

It is well known that in the dilute limit, DLCA process leads to the formation of fractal clusters characterized by a fractal dimension, $D_f \simeq 1.8$. If such an aggregation process is continued for a long time, the system becomes dense and ultimately gels. Several groups in the past have shown similarities between the structure of DLCA clusters near the gel point and percolation clusters. For example, DLCA clusters at the gel point are shown to have the same *large-scale* mass fractal dimension $D_f \simeq 2.6$ as spanning (backbone) percolation clusters [3–5]. A question then naturally arises: how does the DLCA cluster structure cross over from the dilute limit characterized by a fractal dimension of 1.8 to the dense gel state characterized by a fractal dimension of 2.6? Past work was not able to provide a precise answer to this question for the following reason. To study this crossover, one needs to start from a dilute state and follow the evolution of the system for a long time until it becomes crowded and ultimately gels. In contrast, much of the past simulation work has been limited to either (i) small monomer volume fractions f_v carried out for a limited time, so that cluster crowding is yet to substantially modify the cluster morphology or (ii) to high monomer volume fractions [3–5], where the system begins evolving already in a crowded state and any signature of a crossover from dilute to dense is lost. One study in *two dimensions* does address a structural crossover in DLCA clusters [5]. The results, analyzed in real space, show a crossover from the predicted two-dimensional dilute-limit mass fractal dimension to 2d percolation. However, the monomer volume fractions studied were quite large (ranging from 10% to 70%) and the gel-limit structural details were severely limited due to small system sizes. More importantly, no physical explanation was provided as to why such a crossover should exist.

We address this question of *structural crossover* by bridging the gap between dilute and dense regimes in irreversibly aggregating sols through large scale *three-dimensional* simulation of several relevant models. Besides the previously mentioned DLCA model, we also consider both reaction-limited cluster aggregation (RLCA) model and ballistic-limited cluster aggregation (BLCA) model. By starting from a dilute state and allowing the system to evolve until it gels, we clearly demonstrate that the largest cluster develops a hybrid structure with mass fractal dimension $D_f \simeq 2.6$ over large length scales, while at smaller length scales the early time dilute-limit fractal structure, characterized by the particular kinetic model used in the simulation, is frozen in. The largest cluster is thus an aggregate of smaller aggregates with a different fractal dimension, and we call it a "superaggregate." We then show that this crossover in mass fractal dimension occurs at a critical cluster size, which we call the critical radius of gyration. Such a criticality in size has been suggested in previous studies [5–7], vaguely implying a pos-

*Present Address: Polymers Division, National Institute of Standards and Technology, Gaithersburg, MD 20899. Email: dan.fry@nist.gov

sible crossover in structure, but no detailed analysis was given. We, however, explicitly quantify the crossover in structure, in terms of a crossover length scale mentioned above, and provide a physically motivated model of how this length scale depends on monomer volume fraction and mass fractal dimension. In addition, a striking similarity between our DLCA simulation results for the structure factor and static light scattering results in soot clusters is found, both showing $D_f \simeq 2.6$ over large length scales and $D_f \simeq 1.8$ over smaller length scales.

The rest of the paper is organized as follows. We first outline our simulation method. A discussion on how we determine cluster structure in reciprocal and real space and our motivations for focusing on reciprocal space analysis follows. As past simulation work on the sol-gel transition has dealt with diffusion-limited cluster aggregation, we first address the evolution of cluster structure for this type of aggregation and develop a simplified model, giving physical meaning to the newly found structural crossover length scale. To further test the validity of our model and understand this crossover for a broad class of aggregation schemes we follow with simulation results for ballistic-limited and reaction-limited cluster aggregation, comparing the simulated crossover length to our theoretical predictions as a function of mass fractal dimension and polydispersity in cluster size. The "percolationlike" large length scale structure is studied next and contrasted against the spanning backbone cluster from our kinetic models. Subsequently, we compare our results with several experimental studies in colloids and aerosols and conclude with a brief discussion of possibly why this structural crossover has not been seen to date in aggregating colloids.

II. SIMULATION METHOD

In the absence of external forces aggregation of particulate dispersions is governed almost entirely by the relative strengths of attractive and repulsive interactions between the dispersed particles [8]. If the repulsion is entirely suppressed, and the attractive potential negligible except at particle contact, the aggregation rate is limited only by the particle dynamics, which in general is diffusive (random walk) or ballistic (linear trajectory, important in rarified gases). Upon colliding, clusters "stick" together with unit probability P_{stick}. If there is some degree of repulsion, not all collisions result in clusters getting close enough to stick together and $P_{stick} < 1$. Typically, the repulsive barrier E_b between colloidal particles is $\approx 50-100$ MeV [8]. The probability then, at room temperature, that two particles stick together is $P_{stick} = \exp(-E_b/k_BT) \approx 10^{-3}$. With these in mind many physical systems can be separated into essentially three aggregation classes: DLCA, BLCA, and RLCA. We model these three aggregation classes with the following criteria:

(1) DLCA: diffusive cluster motion, $P_{stick}=1$.

(2) BLCA: ballistic (linear trajectory) cluster motion, $P_{stick}=1$.

(3) RLCA: diffusive cluster motion, $P_{stick} \leqslant 10^{-3}$.

In all models presented we assume that the attractive potential is infinite at particle contact, i.e., clusters stick together irreversibly upon colliding.

Using the above listed modeling scheme, we have performed large scale off-lattice Monte Carlo cluster-cluster aggregation simulations for diffusion-limited, ballistic-limited, and reaction-limited aggregation classes in three dimensions. We begin by randomly placing off-lattice N_m monomers in a cubic box of side length L at monomer volume fractions $f_v = 0.0005, 0.001, 0.005, 0.01$, and 0.1. At time $t=0$ the number of clusters is $N_c(0)=N_m$, of size $N=1$ monomer per cluster. The simulation then proceeds by first randomly picking, with probability N_c^{-1}, a cluster of size N. This cluster is moved, with probability N^{-1/D_f}, one monomer diameter in either a randomly chosen direction for the DLCA and RLCA classes, or along a straight line, randomly oriented trajectory for BLCA, where D_f is the well-known dilute-limit mass fractal dimension of a cluster in each respective aggregation class [9–12]. Each time a cluster is picked, the time, measured in Monte Carlo steps per cluster, is incremented by N_c^{-1} regardless of whether the cluster has moved. If two clusters collide the motion is adjusted in order to correct for any overlap between particles and the two stick together with probability P_{stick}.

The functionality with time of the ratio of the nearest-neighbor separation R_{nn} to radius of gyration R_g is $R_{nn}/R_g \propto t^{-z(d-D_f)/dD_f}$, where the kinetic exponent $z>0$ [2]. z is related to the aggregation kernel homogeneity λ, i.e., $z=1/(1-\lambda)$ [13]. Since $D_f < d$ the space dimension, this ratio decreases with time [2,14]. Consequently, the aggregates become increasingly crowded as the system evolves. This is true for all three aggregation classes. The degree of cluster crowding is measured by calculation of the *cluster volume fraction* f_v^c available in the system at time t, where

$$f_v^c(t) = \frac{4\pi}{3L^3}\left(\frac{D_f+2}{D_f}\right)^{3/2}\sum_{i=1}^{N_c(t)} {R_{g,i}}^3. \tag{1}$$

This form for f_v^c uses a reasonable definition of the cluster perimeter radius R_p [15], where

$$R_p^2 = \left(\frac{D_f+2}{D_f}\right)R_g^2. \tag{2}$$

Throughout the results to follow, "dilute" and "dense," or "early" and "late" time corresponds to $f_v^c(t) \ll 1$ and $f_v^c(t) \simeq 1$, respectively. The cluster number, size distribution along with its moments, cluster volume fraction, and radius of gyration are monitored throughout the simulation. The actual gel point is determined by looking for the first system-spanning cluster.

To investigate cluster structure as the system evolves from dilute to dense and ultimately gels, it is important that the clusters are allowed to grow to a size where crowding becomes substantial ($f_v^c \simeq 1$), and yet there are enough clusters left in the system to form a reasonable statistical average. Setting $f_v^c=1$ in Eq. (1), assuming a monodisperse cluster size distribution, fractal clusters ($N \sim R_g^{D_f}$), and the number of clusters at the gel point $N_{c,G} \sim 100$, we estimate the number of monomers needed to see a transition to the dense state. All OLMC simulations presented here have been done at very large system sizes ranging from 8×10^5 to 3×10^6 to

monomers and box sizes L from 162 to 580 monomer diameters $d_m=2a$, where $d_m=1$. All results are an average over 5 or more statistically independent trials.

III. DETERMINATION OF AGGREGATE STRUCTURE

A. Reciprocal space analysis

Light scattering is one of the most frequently used tools for investigating aggregate structure. The intensity of elastically scattered light for a system of N discrete scattering centers can be written as,

$$I(\vec{q}) = NF(\vec{q})S(\vec{q}), \quad q = |\vec{q}| = \frac{4\pi}{\lambda}\sin\left(\frac{\theta}{2}\right), \tag{3}$$

where $S(\vec{q})$ is the static structure factor

$$S(\vec{q}) = \frac{1}{N}\sum_{l,m}^{N} \exp[i\vec{q}\cdot(\vec{r}_l - \vec{r}_m)], \tag{4}$$

$\vec{q}=\vec{k}_f-\vec{k}_i$ is the scattering wave vector, or vector difference between the scattered and incident wave, θ is the scattering angle, and λ the wavelength of light. Because each scattering center is treated as a spherical particle of uniform density, Eq. (4) reduces to

$$S(\vec{q}) = \frac{1}{N}\left|\sum_{l=1}^{N}\exp(i\vec{q}\cdot\vec{r}_\ell)\right|^2 = \frac{1}{N}\left|\sum_{l=1}^{N}(\cos(\vec{q}\cdot\vec{r}_\ell) + i\,\sin(\vec{q}\cdot\vec{r}_\ell))\right|^2, \tag{5}$$

and $F(\vec{q})\rightarrow F(q)$, the well-known form factor for a sphere,

$$F(q) = \left[\frac{3\,\sin(qa) - qa\,\cos(qa)}{(qa)^3}\right]^2. \tag{6}$$

All systems that we model here are isotropic in both cluster position and orientation. We thus perform a spherical average, i.e., $S(\vec{q})\rightarrow S(q)$, by selecting over 100 different $\vec{q}$ values of constant magnitude. This is done by generating the angles (θ,ϕ) according to a uniform differential solid angle $d\Omega$. q is then calculated from,

$$\vec{q} = q_0[\sin(\theta)\cos(\phi)\hat{\mathbf{e}}_1 + \sin(\theta)\sin(\phi)\hat{\mathbf{e}}_2 + \cos(\theta)\hat{\mathbf{e}}_3], \tag{7}$$

where $\hat{\mathbf{e}}_k$ is the kth cartesian unit vector. The most important feature in calculation of $I(q)$ is q itself. It has units of inverse length, and thus probes length scales of q^{-1}. Note that all structural details across length scales larger than the monomer radius a is contained solely in $S(q)$. In the results to follow, we focus on using reciprocal space analysis to study cluster structure. This is motivated by two important observations. (i) the ability to directly compare with light scattering experiments, and (ii) previous work noting that reciprocal space analysis yields structural details that tend to be washed out in real space analysis [16]. However, to be consistent and show that our results are not a product of the method of analysis, we also provide a brief analysis in real space. This analysis method is outlined below.

In results to follow, we focus our attention on the structure of the largest cluster. Reciprocal space analysis for determining the fractal dimension is extremely robust with respect to fluctuations from one simulation run to the next. We explicitly checked this by looking at each individually calculated $S(q)$. Run to run variation in $S(q)$ is negligible except at length scales on the order of the cluster size. Thus one expects that there will be a large statistical variation in calculating the mean cluster size in this way, but we do not use $S(q)$ in this manner. Rather we extract a fractal dimension from the slope of the log-log plot of $S(q)$ vs q, where fluctuations are small. This will be discussed further in Sec. IV.

B. Real space analysis

Overall cluster size can be defined by the radius of gyration

$$R_g{}^2 = \frac{\int r^2\rho(\vec{r})d\vec{r}}{\int \rho(\vec{r})d\vec{r}}, \tag{8}$$

where r is the radial distance measured from the cluster center of mass and $\rho(\vec{r})$ is the position dependent mass density. $\rho(r)$ for a fractal aggregate is well represented at small r by a power law in Ref. [17], i.e., $\rho(\vec{r})=\rho_o r^{D_f-d}$, where d is the space dimension. Cluster mass then scales with geometric size as $M\propto R_g{}^{D_f}$. By plotting $\log(M)$ vs $\log(R_g)$, linear regression yields a slope equal to D_f. For an ensemble of clusters, the value of D_f thus obtained represents an effective fractal dimension over the ensemble, and is not sensitive to the structural details of a single aggregate. Although this method of analysis is appropriate for studying self-similar structure over length scales from the monomer size to the radius of gyration, we have instead chosen to focus on the largest cluster in the system at time t and look for mass scaling by the method of nested spheres [16,18]. For comparison we will also show the effective fractal dimension of the ensemble.

Real space nested spheres analysis of a single cluster is done in the following manner. First, a monomer j is chosen at random from the N monomers in a selected cluster. If it falls within a distance $\delta\equiv|\vec{r}_j-\vec{r}_{cm}|\leqslant\epsilon R_g$, where $\epsilon\leqslant 1$ and $\vec{r}_{cm}$ is the cluster center of mass vector, it becomes the reference center from which all subsequent monomer distances will be measured. Next, we determine the number of monomers m contained within concentric spheres of radius r by summing over all i monomers in the cluster subject to the constraint $|\vec{r}_i-\vec{r}_j|\leqslant r$. r is then incremented by a chosen step size $\Delta r\geqslant d_m$ and the counting process repeated until $m=N$. A new monomer j is then picked again at random from the pool (excluding the previously picked monomers) and the above procedure repeated. Depending on the value of N, we average the entire (r,m) data set over 10 to 100 j values. In this way, the average local structure is probed. Plotting $\log(m)$ vs $\log(r)$ yields a slope equal to D_f. Typically, we have chosen $\epsilon=0.25$ to ensure that cluster edge effects do not contribute to the local structure.

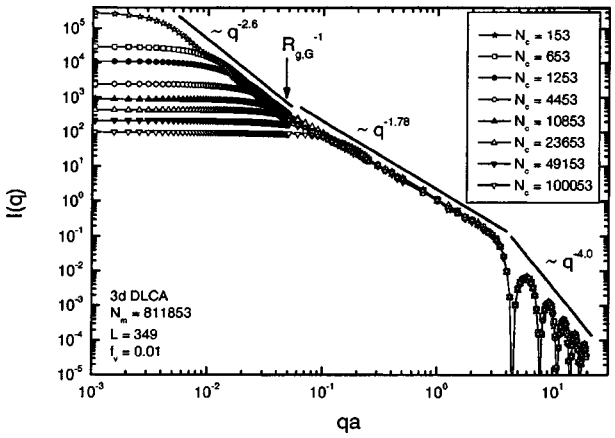

FIG. 1. Structure of the largest cluster is studied by computing $I(q)$ according to Eq. (3) at different times during aggregation for the three-dimensional DLCA simulation with a monomer volume fraction $f_v=0.01$. Here, N_c is the number of clusters at a given time during aggregation. Thus, smaller N_c corresponds to a later time. The location of the calculated ideal gel point radius of gyration [Eq. (11)] is shown as $R_{g,G}^{-1}$. For very large large q, probing the smallest length scale in the system, i.e., the monomer radius a, one observes "interference ripples" and Porod's law $[I(q)\sim q^{-4}]$ in this log-log plot. For intermediate values of q, $I(q)$ characteristic of a DLCA aggregate is seen with a fractal dimension of $D_f\simeq 1.8$ obtained from the slope of the graph. Near the gel point, $I(q)$ evolves to show two power-law regimes. The first regime mentioned above remains intact, but at smaller q, hence at a larger length scale, a $D_f\simeq 2.6$ regime appears. For smaller values of q, the power law gives way to a q-independent Rayleigh regime. Solid lines have been drawn at the designated slope ($\sim q^{-D_f}$) and serve only to guide the eye.

IV. RESULTS AND DISCUSSION

A. Largest cluster structure

1. DLCA Model

In Fig. 1 we show the evolution of the DLCA structure by computing $I(q)$ [Eq. (3)] for the largest cluster with monomer volume fraction $f_v=0.01$. For very large q, probing the smallest length scale in the system, i.e, the monomer radius a, one observes "interference ripples" and Porod's law $[I(q)\sim q^{-4}]$. For intermediate values of q, $I(q)$ shows a power-law behavior $\sim q^{-D_f}$, revealing the well-known dilute-limit DLCA fractal dimension $D_f\simeq 1.8$. For small values of q, the power law gives way to a q independent Rayleigh regime *at earlier times*, where $I(q)=N$ the number of monomers per cluster. The transition between the two regimes is the so-called Guinier regime [19], and determines the cluster size. However, as the system continues to aggregate, forming larger and larger clusters and thus increasing the cluster volume fraction f_v^c, the power-law regime develops yet another slope of ≈ 2.6 at small q, indicating a different fractal dimension at larger length scales. Thus, late in the aggregation process, the largest cluster in the system has a hybrid, inhomogeneous morphology characterized by a short-range *local* structure of $D_f\simeq 1.8$ and a long-range *overall* structure described by $D_f\simeq 2.6$. It is an aggregate composed of aggregates of a different fractal dimension, which we call a "superaggregate." *Moreover, the inflection point in the structure factor suggests another characteristic length scale which separates these two regimes*.

A physical basis to this new length scale can be provided in the following way. Since the fractal dimension of the DLCA aggregates at early times is less than the spatial dimension, when the aggregation proceeds to a certain *critical size*, the aggregates will fill the volume by barely touching each other and the system will gel. To calculate this critical size we assume the system to be made of equal sized spherical clusters. We take the monomer volume fraction of an individual cluster $f_{v,i}$ to be

$$f_{v,i}=\frac{Na^3}{(4\pi/3)R_p^3}, \tag{9}$$

where N is the number of monomers per cluster and the cluster perimeter radius is given by Eq. (2). We also use the fundamental relation

$$N=k_0\left(\frac{R_g}{a}\right)^{D_f}. \tag{10}$$

Past work has shown that $k_0\simeq 1.3$ for the DLCA aggregation class [20]. Our present findings yield a similar value as well and $k_0\simeq 1.4, 1.2$ for BLCA and RLCA, respectively. The condition that the clusters have grown to fill the entire system volume means that the monomer volume fraction of an individual cluster $f_{v,i}$ is equal to the fixed monomer volume fraction of the entire system f_v, $f_{v,i}=f_v$. Using Eqs. (2), (9), and (10), we solve to find R_g when this happens:

$$R_{g,G}=a\left[k_0^{-1}\left(\frac{D_f+2}{D_f}\right)^{d/2}f_v\right]^{-1/(d-D_f)}. \tag{11}$$

We call this the *ideal* gel point radius of gyration.

We show in Fig. 1 the location of $R_{g,G}^{-1}$ calculated from Eq. (11). This coincides with the inflection point in $I(q)$ providing a strong support to the physical picture described above. Of course, in real situations, the substructures that build the gel structure are neither spherical nor monodisperse.

Equation (11) shows a strong dependence of $R_{g,G}$ on monomer volume fractions f_v. To test this functional dependence, we investigate the structure of the largest DLCA cluster as a function of time for another monomer volume fraction $f_v=0.1$. Results are shown in Fig. 2. A similar crossover from $D_f\simeq 1.8$ to $D_f\simeq 2.6$ is seen again at a crossover length scale which matches extremely well with a smaller value of $R_{g,G}$ corresponding to this higher volume fraction.

We would like to point out that results for $f_v=0.0005, 0.001, 0.005$ showed either no gel point over our simulation time or a gel point at such late times that the apparent crossover length was near the box size L. If $L\simeq R_{g,G}$, clusters cannot grow large enough for the second large length scale structure to develop. Reaching the gel point for $f_v=0.0005$ required $N_m\geqslant 10^7$, inaccessible by current computational methods. Thus we have only shown results for $f_v=0.01, 0.1$, but note that $f_v=0.01$ is at least an order of magnitude less than monomer volume fractions studied in past simulations.

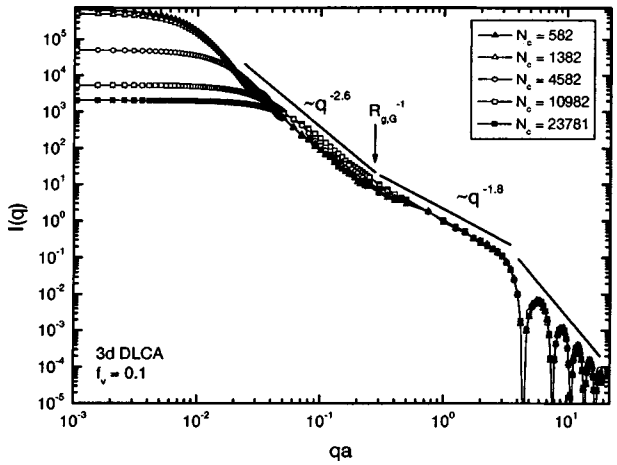

FIG. 2. Same as in Fig. 1 except for a monomer volume fraction $f_v=0.1$. A crossover from $D_f \simeq 1.8$ to $D_f \simeq 2.6$ is seen again at a crossover length scale which matches extremely well with a smaller value of $R_{g,G}$ corresponding to this higher volume fraction. Solid lines have been drawn at the designated slope ($\sim q^{-D_f}$) and serve only to guide the eye.

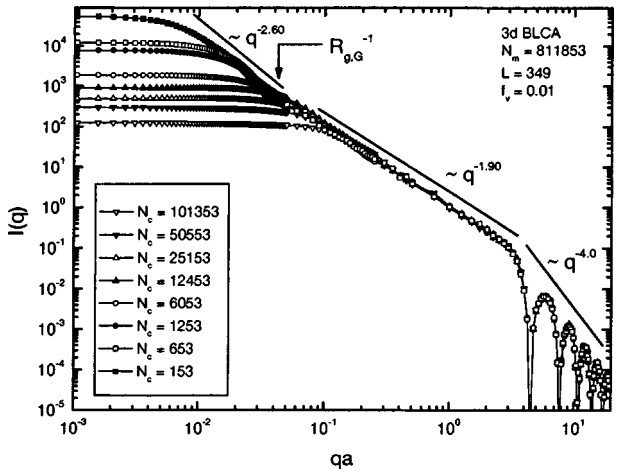

FIG. 3. Same as in Fig. 1 except for the three-dimensional BLCA model. Both a Porod regime and a q-independent Rayleigh regime are present as seen in the DLCA results (Fig. 1). For intermediate values of q, $I(q)$ shows a power-law behavior mq^{-D_f}, revealing the well-known dilute-limit BLCA fractal dimension $D_f \simeq 1.9$. However, the second power-law regime, characterized by another slope of ≈ 2.6 (seen in Fig. 1 at late times) and starting at an inflection point given by $R_{g,G}^{-1}$ is less pronounced in this figure. Solid lines have been drawn at the designated slope ($\sim q^{-D_f}$) and serve only to guide the eye.

2. BLCA and RLCA Models

It is known that clusters produced under reaction-limited conditions are more polydisperse in size than their diffusion-limited counterparts [21]. Likewise, predictions for the ballistic-limited scenario yield a polydispersity greater than DLCA but substantially less than what is found for RLCA. Since an inherent assumption made in our definition of $R_{g,G}$ is that of a monodisperse cluster size distribution, it is reasonable to question its validity as a descriptor of the crossover length in systems where the cluster size distribution is very polydisperse. Moreover, since the large length scale structure near the gel point of DLCA model is characterized by a different fractal dimension $D_f \simeq 2.6$, it is natural to ask whether a similar gel point fractal dimension would be present in clusters formed by other kinetic models such as BLCA and RLCA. For these reasons, we have also performed large-scale simulations for the BLCA and RLCA models in three dimensions. The corresponding structure of the largest cluster for monomer volume fraction $f_v=0.01$ is shown in Figs. 3 and 4.

Similar to the DLCA case, one observes "interference ripples" and Porod's law [$I(q) \sim q^{-4}$] for very large q probing the monomer size. For intermediate values of q, $I(q)$ shows a power-law behavior $\sim q^{-D_f}$, revealing the well-known dilute-limit BLCA ($D_f \simeq 1.9$) and RLCA structure ($D_f \simeq 2.1$) in Figs. 3 and 4, respectively. As before, for small values of q, the power law gives way to a q-independent Rayleigh regime *at earlier times*. However, the second power-law regime, seen at late times in Fig. 1 and characterized by a slope of ≈ 2.6 is less pronounced in BLCA and RLCA. The inflection point in $I(q)$ at $R_{g,G}^{-1}$ is also quite weak. Because RLCA clusters are less ramified than DLCA clusters, they have to grow to a larger $R_{g,G}$ ($N \sim R_g^{D_f}$) in order to form a superaggregate. Due to the finite simulation size, RLCA does not reach this point for $f_v=0.01$ until near the end of the simulation. To remedy this we need to go to higher f_v and thus to a lower value of $R_{g,G}$, or more importantly for a finite system, lower value of $R_{g,G}/L$.

Such simulations for BLCA and RLCA with $f_v=0.1$ are carried out, and the results are shown in Figs. 5 and 6, respectively, for the largest cluster as a function of time. As

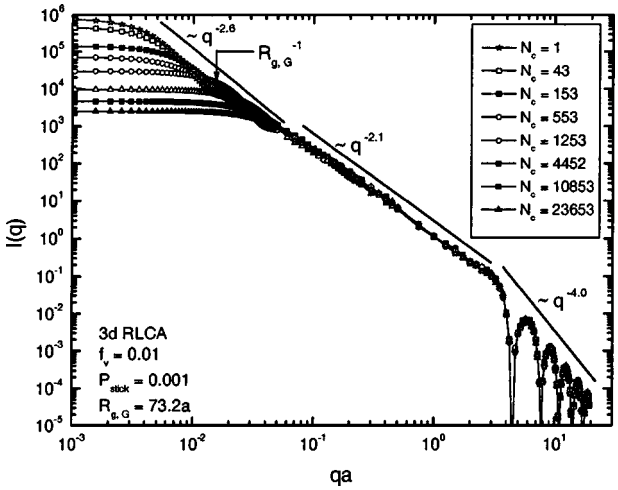

FIG. 4. Same as in Fig. 1 except for the three-dimensional RLCA model. Both a Porod regime and a q-independent Rayleigh regime are present as seen in the DLCA results (Fig. 1). For intermediate values of q, $I(q)$ shows a power-law behavior mq^{-D_f}, revealing the well-known dilute-limit RLCA fractal dimension $D_f \simeq 2.1$. However, the second power-law regime, characterized by another slope of ≈ 2.6 (seen in Fig. 1 at late times) and starting at an inflection point given by $R_{g,G}^{-1}$ is less pronounced in this figure. Solid lines have been drawn at the designated slope ($\sim q^{-D_f}$) and serve only to guide the eye.

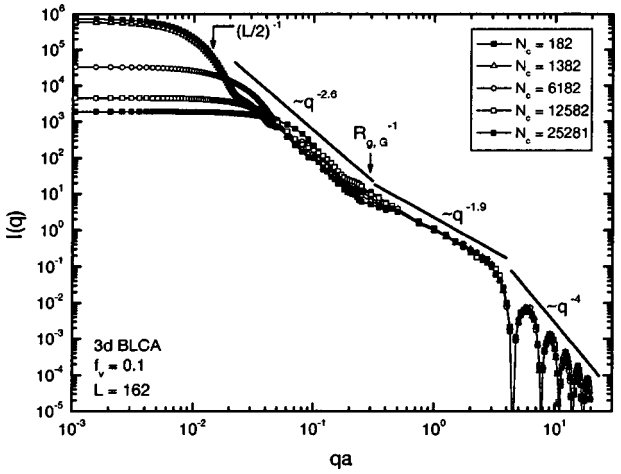

FIG. 5. Same as in Fig. 3 except for a monomer volume fraction $f_v=0.1$. Development of the second power-law regime at late times, characterized by another slope of ≈ 2.6 and starting around an inflection point given by $R_{g,G}^{-1}$ is clear for this BLCA simulation. Solid lines have been drawn at the designated slope ($\sim q^{-D_f}$) and serve only to guide the eye.

can be clearly seen in these figures, BLCA and RLCA simulations show, at smaller length scales (large q), a fractal dimension of 1.9 or 2.1, respectively. More importantly, a model independent large-scale (small q) fractal dimension of 2.6 develops at late times, consistent with the DLCA model. This implies, within the scatter of our data [22], that the aggregate of aggregates, or superaggregate, has a *large scale* structure independent of the prescribed kinetic model. The hybrid nature of the superaggregate is also clear: a different fractal dimension, characterized by the underlying aggregation kinetics, is also observed but only over length scales smaller than the ideal gel point radius of gyration.

In Fig. 7 we show the measured crossover length from the simulations, which we denote as $(q_c)^{-1}$, as a function of the

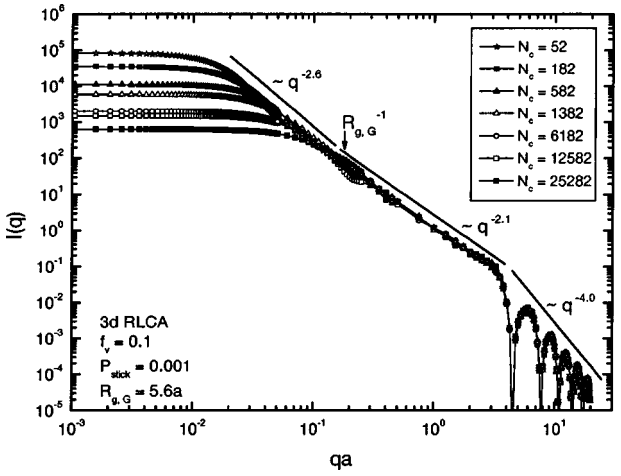

FIG. 6. Same as in Fig. 4 except for a monomer volume fraction $f_v=0.1$. Development of the second power-law regime at late times, characterized by another slope of ≈ 2.6 and starting around an inflection point given by $R_{g,G}^{-1}$ is clear for this RLCA simulation. Solid lines have been drawn at the designated slope ($\sim q^{-D_f}$) and serve only to guide the eye.

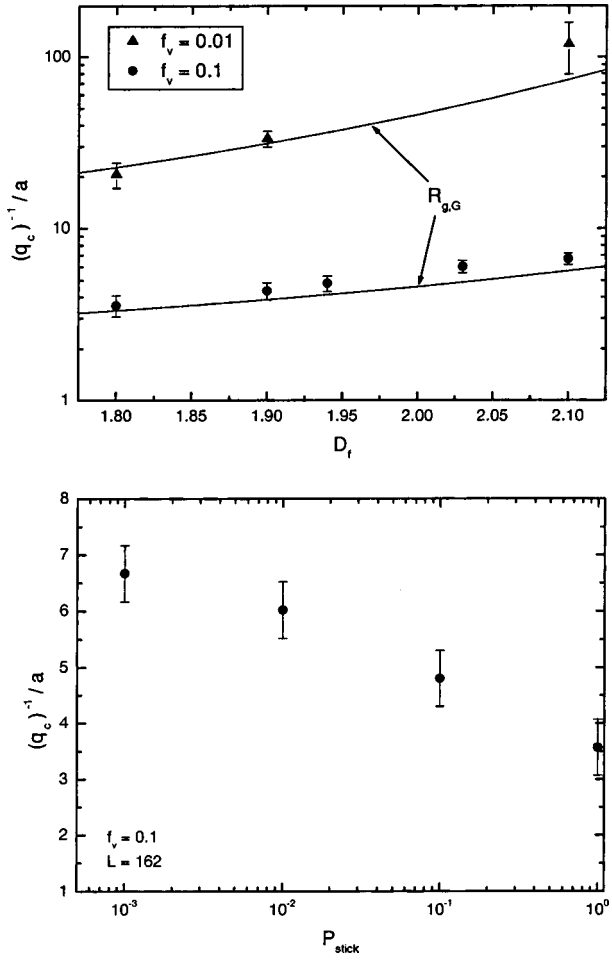

FIG. 7. Measured crossover length scale $(q_c)^{-1}$ as a function of mass fractal dimension D_f and sticking probability P_{stick}. D_f has been determined from a linear least squares fit of $ln(N)$ vs $ln(R_g/a)$ in the dilute limit (early time). Error in $(q_c)^{-1}$ was estimated by looking at variations in slope from a least squares fit of the two power-law regimes near the crossover length in q space. According to our predictions [Eq. (11)], $(q_c)^{-1}=R_{g,G}$. A comparison between the measured $(q_c)^{-1}$ and $R_{g,G}$ is shown in the top figure. The bottom figure is a measure of how much the cross over length scale shifts to larger values as a function of the sticking probability. Note that $P_{stick}=1$ corresponds to the diffusion-limited aggregation class.

dilute-limit fractal dimension (top) and sticking probability P_{stick} (bottom). $R_{g,G}$ [Eq. (11)] is a function of both D_f and f_v. Thus we plot (shown as solid lines) $R_{g,G}$ as a function of D_f at fixed f_v for $f_v=0.01$, 0.1. Data points at $D_f \simeq 1.8$, 1.9, 2.1 correspond to the DLCA, BLCA, and RLCA simulation results, respectively. The two intermediate points between BLCA and RLCA correspond to RLCA simulations with $P_{stick}=0.1, 0.01$. We first note (see bottom of Fig. 7) that $(q_c)^{-1}$ is not a strong function of P_{stick}. q_c^{-1} increases only by a factor of ~ 2 from the limiting DLCA value at $P_{stick}=1$ to $P_{stick}=0.001$. Second, the agreement between $(q_c)^{-1}$ and the predicted $R_{g,G}$ is quite good considering the assumption of spherical clusters and a monodisperse cluster size distribution used in deriving $R_{g,G}$. The measured $(q_c)^{-1}$ follow the same trend as the predicted curve, but all data fall systematically above $R_{g,G}$. The slight disagreement between the two

becomes worse with increasing D_f. As mentioned above, RLCA is more polydisperse in cluster size than both DLCA and BLCA with DLCA being the least polydisperse. It thus appears that increasing polydispersity pushes the crossover length to a *slightly higher value* than that predicted from $R_{g,G}$ which is defined assuming a monodisperse distribution.

B. Comparison with backbone percolation clusters

What is the significance of the slope of magnitude 2.6 at large length scales in the OLMC results? This indicates a mass fractal dimension of $D_f \simeq 2.6$, very close to the accepted mass fractal dimension D_f for a percolating backbone in three-dimensions , and in agreement with other simulation results of the sol-gel transition [4]. Before comparing our results with percolation though, a few comments are in order. One intuitively expects that the aggregation and percolation models have drastically different properties, in part because the former is *dynamic* and the latter *static*, but more so because percolation represents a state of criticality and aggregation models do not. Indeed different properties are found when comparing cluster size distributions and corresponding scaling laws (for instance, see Ref. [18] for percolation scaling laws and Fig. 17 of Ref. [3] for a comparison of scaling in percolation and DLCA; for a full discussion of dilute-limit cluster size distribution scaling laws see Ref. [14]). However, for aggregating models, a critical behavior develops at the sol-gel transition and this transition has a lengthy history of being compared to percolation, via the mass fractal dimension [3,5,23–26]. Percolation clusters can be characterized by a range of fractal dimensions, describing both mass and surface structure. We choose however, to address the "percolation-like" behavior of the spanning cluster in the OLMC only through the mass fractal dimension. Although this is not a complete analysis in the strict sense, it is the mass fractal dimension which yields structural details through light scattering measurements.

Since the large-scale mass fractal dimension of the largest cluster near the gel point is almost identical to the mass fractal dimension of a percolating backbone, we propose a picture of sol-gel transition in irreversibly aggregating systems. A dilute sol aggregates via DLCA, RLCA, or BLCA kinetics yielding aggregates with fractal dimensions of 1.8 or 2.1, or 1.9, respectively. Because these aggregate fractal dimensions are less than the spatial dimension, the effective aggregate volume fraction (the occupied volume of the aggregates normalized by the system volume) approaches unity as the aggregation proceeds. At the ideal gel point, the aggregates are so crowded that they percolate to form a superaggregate made up of fractal aggregates with an average size of $R_{g,G}$.

Instead of the traditional percolation scenario of statically placing particles on lattice (site percolation) or off lattice (continuum percolation), at increasingly larger monomer volume fractions until a spanning cluster is formed, aggregating systems forming fractal-like clusters eventually percolate due to an increasing cluster volume fraction f_v^c as the system evolves. This implies that the largest cluster is formed by the percolation of smaller clusters, each with a dilute-limit fractal morphology. Further support for this picture comes from noting that the large length scale fractal dimension, $D_f \simeq 2.6$, is practically independent (within the scatter of our data) of the kinetic model used to produce such a cluster. It is only at small length scales, below the critical radius of gyration, that the prescribed kinetic model dictates cluster structure.

To further analyze the similarity and difference between kinetically grown clusters at the gel point and static percolation backbone, we have performed three-dimensional percolation simulations. We limit ourselves to site percolation since all percolation models yield mass fractal dimension $D_f \simeq 2.55$ [18]. Sites on a simple cubic lattice of side length $L=256$ and lattice spacing $\ell = d_m = 1$, were populated with probability $p=p_c \simeq 0.31$ [18], where d_m is the monomer diameter and p_c the percolation threshold. The backbone cluster was then isolated and $I(q)$ calculated according to Eq. (3).

Results, averaged over 10 statistically independent trials, are shown in Fig. 8. The q axis is scaled by $R_{g,G}$; $qR_{g,G}=1$ corresponds to scattering which probes length scales on the order of $R_{g,G}$. For the percolation simulation $R_{g,G}=a$ the monomer radius. We find that $I(q)$ has a power-law regime with exponent $D_f \simeq 2.5$, verifying the archetypical percolation backbone mass fractal structure. At $qR_{g,G}=1$, $I(q)$ crosses over to the well-known spherical particle form factor. This crossover at the monomer length scale is expected and is also seen in the OLMC results (Figs. 1–6). This is, however, not the crossover of interest. We also show in Fig. 8 $I(q)$ of the gel point largest cluster for DLCA at $f_v=0.01$. At low q results show a power-law behavior with $D_f \simeq 2.5$, as similarly found for the percolation backbone and also shown in Fig. 1. We must stress here that although this structure has been previously seen in simulation, it was never discussed as to over which length scale it occurs, nor how it develops. The q axis is again scaled by $R_{g,G}$, but we now use the predicted ideal gel point radius of gyration for DLCA at this monomer volume fraction, given by Eq. (11). At $qR_{g,G}=1$, $I(q)$ shows an inflection to yet another power-law regime with smaller slope ca. $\simeq 1.8$, the dilute-limit mass fractal dimension for DLCA clusters. This clearly supports our proposed picture of how, structurally, the sol-gel transition proceeds. Individual dilute-limit clusters act as "monomers" in the percolation scenario. Instead of the monomeric structure being dictated by the spherical form factor, each effective site now has a structure dictated by the prescribed kinetic model when dilute. In irreversibly aggregating systems the early time structure becomes frozen within the percolated network. This hybrid or "*biphase*" structure in mass fractal dimension sets the largest cluster apart from the archetypical percolation backbone. Since our analysis is given in terms of the mass fractal dimension, it is amenable to experimental verification from light scattering data.

Further comparison with percolation can be made by probing the cluster-ensemble averaged structure. Static percolation systems at the percolation threshold are known to consist of a backbone with $D_f \simeq 2.55$ and smaller clusters, known as lattice animals, with $D_f \simeq 1.9$. We can probe the difference in the ensemble averaged D_f between the kinetic OLMC and static percolation by plotting $\log(N)$ versus

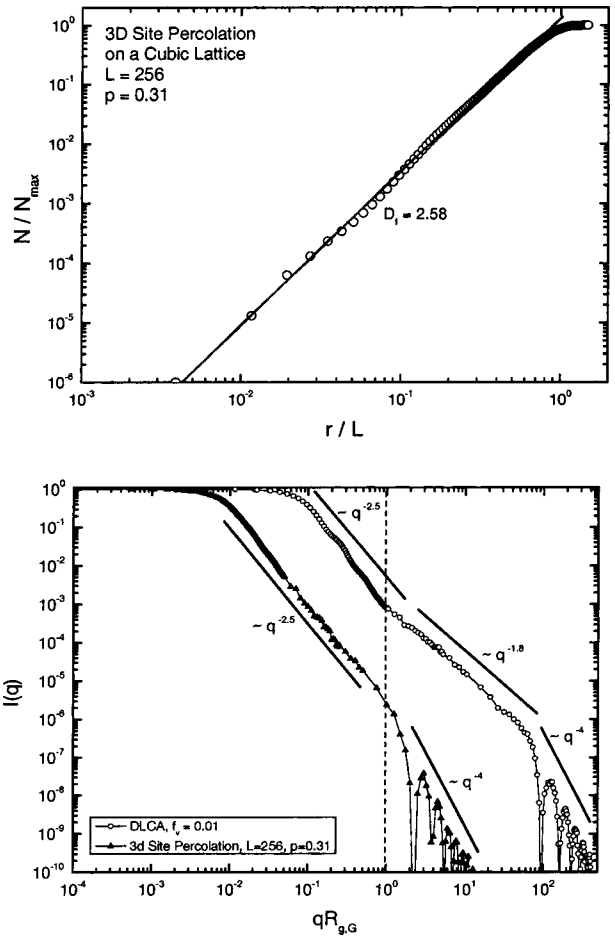

FIG. 8. (Top) Three-dimensional site percolation backbone structure at $p=p_c$. The top graph shows the real space analysis using the method of concentric circles. The solid line is a result of performing a least squares fit over the range $0.01 \leqslant r/L \leqslant 0.4$. (Bottom)The bottom graph shows the q-space structure represented by $S(q)$ and calculated according to Eq. (5). To directly compare with the DLCA largest cluster results, we have scaled the horizontal axis by $R_{g,G}$ such that $qR_{g,G}=1$. For site percolation $R_{g,G}=a$. With DLCA, we have used $R_{g,G}$ calculated according to Eq. (11), with $D_f=1.8$ and $f_v=0.01$. Solid lines have been drawn at the designated slope ($\sim q^{-D_f}$) and serve only to guide the eye.

$\log(R_g)$ for the ensemble of clusters. Results are shown in Fig. 9. The solid lines are from a linear least squares fit yielding a slope of D_f. These two values are quite different, and imply different distributions of D_f amongst the ensemble in these two systems. Although there are similarities between the largest cluster and the backbone of static percolation, the ensemble of clusters in the OLMC at the gel point and static percolation is structurally different.

C. Comparison with experiment

It is well established that soot in diffusion flames aggregates under DLCA conditions [27]. The advantage to studying aggregation in a sooty flame is that the aggregation time is coupled to the height above the flame burner allowing different aggregation times to be easily probed. We have performed measurements of aggregate structure in an acetylene (C_2H_2)/air diffusion flame, using static light scattering [28]. The scattered light intensity $I(q)$ was measured as a function of height above the burner. Results are shown as $S(q)$ in Fig. 10.

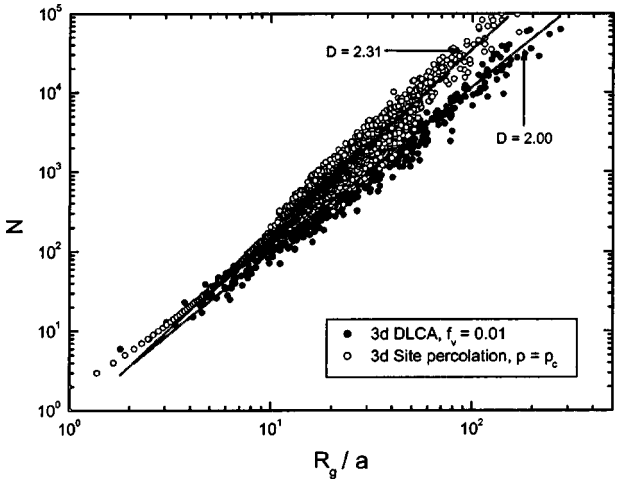

FIG. 9. Comparison of mass scaling for the ensemble of clusters between three-dimensional DLCA at the gel point and three-dimensional site percolation at the percolation threshold. Solid lines are from performing a linear least squares fit.

At early time, and low heights in the flame, we find typical DLCA soot clusters with $D_f \simeq 1.8$. The power-law regime gives way at $q^{-1} \simeq R_g$ to a q independent Rayleigh regime. However, with increasing height above the burner, an increased intensity at low q develops, marked by a second power-law regime with slope $D_f \simeq 2.6$. Is this second structure then due to crowding and subsequent percolation of clusters within the flame?

Over the range of heights measured, the flame narrows. At low height the measured f_v with $D_f=1.8$ yields an $R_{g,G}$ well out of range of the observed $(q_c)^{-1}$. However, at larger heights, assuming mass conservation, the narrowing of the

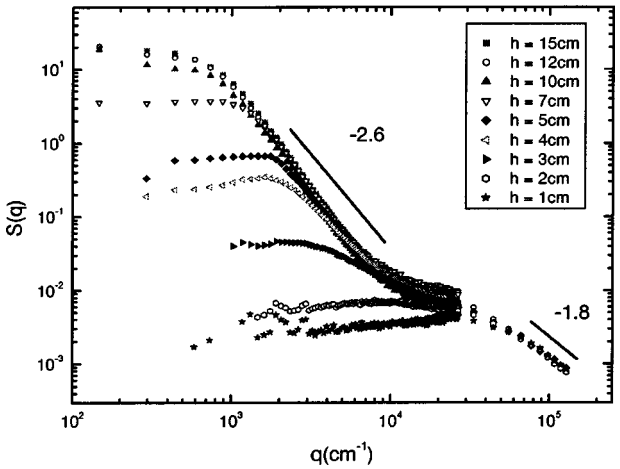

FIG. 10. Scattered light intensity from a C_2H_2/air flame at different height above the burner. Results from Sorensen *et al.* [28]. Solid lines are have been drawn at the designated slope ($\sim q^{-D_f}$) and serve only to guide the eye.

flame results in a larger f_v. This yields a value of $R_{g,G}$ in reasonable agreement with (q_c^{-1}), implying that what we observe in simulation is happening in the sooting flame. We note however, that shear forces, possibly present in the flame, could cause the clusters to restructure and thus raise D_f. Although the experimental and simulation results appear to have good agreement, this needs to be ruled out before a definitive conclusion can be made.

Studies of gel structure are vast and numerous. For instance, structure of latex, polystyrene, and particulate silica and gold dispersions have been intensely investigated, via static light scattering, near the gel point within the past 25 years [29–36]. Interestingly, none has shown a crossover to percolation, and many conclude that the gel structure is well described by either the DLCA or RLCA models. We have used the values of f_v from these past studies to calculate $R_{g,G}$ and compare $R_{g,G}^{-1}$ with the small q range of the measured light scattering data. Of these, most light scattering spectra were cut off either prior to reaching $q=R_{g,G}^{-1}$, or within a factor of 2 beyond $R_{g,G}^{-1}$. Several studies extended the q range approximately one order of magnitude beyond $R_{g,G}^{-1}$ but the systems appeared to be either in the RLCA regime or were at such a high monomer volume fraction that the monomers themselves percolated. Our results imply that cluster growth a few orders of magnitude beyond $R_{g,G}$ may be necessary in RLCA systems in order to see the crossover.

Fragmentation may also be present in real systems. Because fragmentation does not occur over any specific length scale where the monomer coordination number is low, repeatedly breaking the clusters may wash out the crossover length. Moreover, colloidal particles typically interact with finite magnitude over length scales of one to several particle diameters, where DLCA assumes infinite attraction at contact. Past work has shown that depending on the magnitude and range of the interaction potential the percolation threshold increases or decreases [37,38].

Several studies have reported on an increase in mass fractal dimension in gelled suspensions, but attribute the change to either restructuring due to aging, or direct inclusion of restructuring at the monomer level within the simulation details [39–41]. Moreover, restructuring results in an increased mass fractal dimension over the entire cluster length scale, i.e., there is no crossover length beyond the monomer size. Our algorithm does not incorporate aging or restructuring, and thus the new structure and location in q space can only result from the prescribed kinetic model by which the system evolves.

V. CONCLUSIONS

We have simulated cluster-cluster aggregation for the diffusion-limited (DLCA), ballistic-limited (BLCA), and reaction-limited (RLCA) aggregation classes, and covering three orders of magnitude of monomer volume fraction f_v. At early time, when dilute as measured by the cluster volume fraction f_v^c, we find archetypical solid particle clusters of $D_f \simeq 1.8, 1.9, 2.1$ for DLCA, BLCA, and RLCA, respectively. As the system evolves and becomes dense $(f_v^c \to 1)$, the largest cluster in the systems develops a two-phase *hybrid* morphology characterized by a fractal dimension ca. 2.6 over large length scales, independent (within the scatter of our data) of aggregation class, and a smaller fractal dimension at small length scales. We find that the small length scale morphology of the largest cluster is equivalent to the dilute-limit small cluster morphology, which is dependent on aggregation class. This suggests that the largest cluster is an aggregate of smaller aggregates. We call this large cluster a "superaggregate."

Our simulation results provide a picture of how the sol-gel transition proceeds structurally. A dilute sol aggregates via DLCA, RLCA, or BLCA kinetics yielding aggregates with fractal dimensions of 1.8, 2.1, or 1.9, respectively. At the ideal gel point, the aggregates are so crowded that they percolate to form a superaggregate made up of fractal aggregates with an average size of $R_{g,G}$. This scenario of how the spanning cluster forms in simulations of aggregating sols is new to our work. The simulated DLCA length scale marking the crossover between the two morphologies, termed the critical radius of gyration, is in good agreement with a calculation based on a monodisperse cluster size distribution. BLCA and RLCA simulation results, where polydispersity in cluster size is larger than DLCA, show a crossover length scale systematically larger than the monodisperse prediction. We find qualitative agreement between our simulation results and experimental results of aggregating soot clusters.

ACKNOWLEDGMENTS

Financial support was given by NASA grant Grant No. NAG 3-2360 and NSF grant Grant No. CTS080017.

[1] J. E. Martin and D. Adolf, Annu. Rev. Phys. Chem. **42**, 311 (1991).
[2] D. Fry, T. Sintes, A. Chakrabarti, and C. M. Sorensen, Phys. Rev. Lett. **89**, 148301 (2002).
[3] J. C. Gimel, D. Durand, and T. Nicolai, Phys. Rev. B **51**, 11348 (1995).
[4] J. C. Gimel, T. Nicolai, and D. Durand, J. Sol-Gel Sci. Technol. **15**, 129 (1999).
[5] A. Hasmy and R. Jullien, Phys. Rev. E **53**, 1789 (1996).
[6] W. C. K. Poon and M. D. Haw, Adv. Colloid Interface Sci. **73**, 71 (1997).
[7] J. Bibette, T. G. Mason, H. Gang, and D. A. Weitz, Phys. Rev. Lett. **69**, 981 (1992).
[8] R. Hunter, *Foundations of Colloid Science* (Clarendon Press, Oxford, 1987).
[9] D. A. Weitz and M. Oliveria, Phys. Rev. Lett. **52**, 1433 (1984).
[10] A. Hasmy, M. Foret, J. Pelous, and R. Jullien, Phys. Rev. B **48**, 9345 (1993).

[11] D. A. Weitz, J. S. Huang, M. Y. Lin, and J. Sung, Phys. Rev. Lett. **54**, 1416 (1985).
[12] M. Y. Lin, H. M. Lindsay, D. A. Weitz, R. C. Ball, R. Klein, and P. M. Meakin, Phys. Rev. A **41**, 2005 (1990).
[13] S. K. Friedlander, *Smoke, Dust and Haze* (Oxford, New York, 2000).
[14] C. Oh and C. M. Sorensen, J. Aerosol Sci. **28**, 937 (1997).
[15] C. Oh and C. M. Sorensen, J. Colloid Interface Sci. **193**, 17 (1997).
[16] C. Oh and C. M. Sorensen, Phys. Rev. E **57**, 784 (1998).
[17] R. Julien and R. Botet, *Aggregation and Fractal Aggregates* (World Scientific, Singapore, 1987).
[18] D. Stauffer and A. Aharony, *Introduction to Percolation Theory* (Taylor&Francis, London, 1985).
[19] A. Guinier, G. Fournet, C. B. Walker, and K. L. Yudowitch, *Small Angle Scattering of X-Rays* (Wiley, New York, 1955).
[20] C. M. Sorensen and G. Roberts, J. Colloid Interface Sci. **186**, 447 (1997).
[21] D. J. Robinson and J. C. Earnshaw, Phys. Rev. Lett. **71**, 715 (1993).
[22] We point out here that the deviation between the line of slope $D_f=-2.6$ and simulation results near the bend at low q is due to large fluctuations in superaggregate size. The power law regime at higher q however, where we determine $D_f \simeq 2.6$, is robust with respect to run-to-run fluctuations. We have explicitly checked this and find only a 6% error in D_f obtained by performing a linear regression in the power law regime.
[23] M. Kolb and H. J. Herrmann, J. Phys. A **18**, L435 (1985).
[24] H. J. Herrmann and M. Kolb, J. Phys. A **19**, L1027 (1986).
[25] M. Kolb, J. Phys. A **19**, L263 (1986).
[26] P. Jensen, P. Melinon, A. Hoareau, J. X. Hu, B. Cabaud, M. Treilleux, E. Bernstein, and D. Guillot, Physica A **185**, 104 (1992).
[27] C. M. Sorensen and G. D. Feke, Aerosol Sci. Technol. **25**, 328 (1996).
[28] C. M. Sorensen, W. Kim, D. Fry, D. Shi, and A. Chakrabarti, Langmuir **19**, 7560 (2003).
[29] R. Vacher, T. Woignier, J. Pelous, and E. Courtens, Phys. Rev. B **37**, 6500 (1988).
[30] J. E. Martin and J. P. Wilcoxon, Phys. Rev. A **39**, 252 (1989).
[31] F. Ferri, B. Frisken, and D. Cannell, Phys. Rev. Lett. **67**, 3626 (1991).
[32] M. Carpinetti and M. Giglio, Phys. Rev. Lett. **68**, 3327 (1992).
[33] B. J. Frisken, D. S. Cannell, M. Y. Lin, and S. K. Sinha, Phys. Rev. E **51**, 5866 (1995).
[34] M. Kroon, W. L. Vos, and G. H. Wegdam, Phys. Rev. E **57**, 1962 (1998).
[35] P. Varadan, M. J. Solomon, Langmuir **17**, 2918 (2001).
[36] J. E. Martin, J. Wilcoxon, and D. Adolf, Phys. Rev. A **36**, 1803 (1987).
[37] S. A. Safran, I. Webman, and G. S. Grest, Phys. Rev. A **32**, 506 (1985).
[38] A. L. R. Bug, S. A. Safran, and G. S. Grest, Phys. Rev. Lett. **55**, 1896 (1985).
[39] L. Cipelletti, S. Manley, R. C. Ball, and D. A. Weitz, Phys. Rev. Lett. **84**, 2275 (2000).
[40] R. Jullien, A. Hasmy, and E. Anglaret, J. Sol-Gel Sci. Technol. **8**, 819 (1997).
[41] P. Marsh, G. Bushell, and R. Amal, J. Colloid Interface Sci. **241**, 286 (2001).